ACS APPLIED MATERIALS & INTERFACES

Research Article

www.acsami.org

Effect of Methanol Addition on the Resistivity and Morphology of PEDOT:PSS Layers on Top of Carbon Nanotubes for Use as Flexible Electrodes

Weijia Wang,[†] Matthias A. Ruderer,[†] Ezzeldin Metwalli,[†] Shuai Guo,[†] Eva M. Herzig,[‡] Jan Perlich,[§] and Peter Müller-Buschbaum*[,†]

[†]Physik-Department, Lehrstuhl für Funktionelle Materialien, Technische Universität München, James-Franck-Straße 1, 85748 Garching, Germany

[‡]Munich School of Engineering, Herzig Group, Technische Universität München, Lichtenbergstraße 4, 85748 Garching, Germany

[§]Deutsches Elektronen-Synchrotron (DESY), Notkestraße 85, 22603 Hamburg, Germany

ABSTRACT: Overcoating carbon nanotube (CNT) films on flexible poly(ethylene terephthalate) (PET) foils with poly(3,4-ethylenedioxythiophene):poly(styrenesulfonate) (PEDOT:PSS) layers reduces the surface roughness, which is interesting for use in organic electronics. Adding methanol to the PEDOT:PSS aqueous solution used for spin coating of the PEDOT:PSS layer improves the wetting behavior of the CNT/PET surface. Samples with different volume fractions of methanol (0, 33, 50, 67, and 75 vol %) are compared with respect to the transmission, horizontal, and vertical resistivity. With grazing-incidence small-angle X-ray scattering, the film morphologies are probed, which is challenging because of the substrate flexibility. At 50 vol %, methanol optimum conditions are achieved with the resistivity close to that of the bare CNT/PET substrates because of the best contact between the PEDOT:PSS film and CNT surface. At lower methanol ratios, the PEDOT:PSS films cannot adapt the CNT morphology, and at higher methanol ratios, they rupture into domains and no continuous PEDOT:PSS layers are formed.

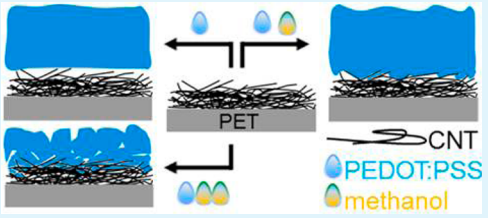

KEYWORDS: *PEDOT:PSS, flexible electrodes, GISAXS, morphology, resistivity*

1. INTRODUCTION

In the last decades, organic electronic devices such as, for example, touch screens, organic light-emitting diodes (OLEDs), organic photodiodes, and organic photovoltaic (OPV) devices have received very high attention. Advantages such as the use of lightweight materials, the possibility of low-energy solution processing, and potential low costs in conjunction with novel possibilities, which arise from the flexibility and the possibility of tuning the shape and color, render them highly interesting.[1−9] Meanwhile, for example, power conversion efficiencies of OPV devices have exceeded 10%, which makes organic solar cells potential alternatives to traditional silicon solar cells.[10,11] This increases interest in fabricating organic solar cells on flexible substrates and on large scales.[12−14] The same holds for the rather further developed devices such as touch screens, OLEDs, and organic photodiodes. Therefore, flexible transparent substrates and electrodes are required. For use in flexible organic electronics, substrates such as poly(ethylene terephthalate) (PET) or poly(ethylene 2,6-naphthalate) (PEN) are promising candidates to replace rigid glass substrates.[15] In rigid organic electronic devices such as, for example, OPV devices, the conventional anode material used is commonly indium−tin oxide (ITO) because of its high conductivity and transmission.[16,17] However, the worldwide available amount of indium is extremely rare, and therefore the use of ITO will make a mass production of OPV devices very cost-intensive. Moreover, ITO electrodes crack easily when bent or strained.[18−20] Both drawbacks of ITO electrodes limit their application in large-scale and flexible organic electronics. As a consequence, new flexible electrode materials are critical. Presently, highly conductive poly(3,4-ethylenedioxy thiophene):poly(styrenesulfonate) (PEDOT:PSS) and carbon nanotube (CNT) films are being identified as potential candidates to replace ITO electrodes because they have a similar work function (4.5−5.2 eV for the CNT film and 4.9−5.2 eV for the PEDOT:PSS film) compared with ITO electrodes (4.4−4.9 eV).[21−23] Moreover, both PEDOT:PSS and CNT films offer advantages such as good optical transmission, excellent electronic properties, element abundance, low cost, and mechanical flexibility.[24−27] However, on the basis of different applications, CNT films provide unique properties compared to highly conductive PEDOT:PSS films. The CNT films exhibit similar transparency over the entire visible-wavelength range, which is beneficial for OLEDs, touch screens, and OPV applications. Moreover, CNT films exhibit higher tensile strength and Young's modulus, both being beneficial for the mechanical behavior required in flexible devices.[28] Consequently, flexible organic electronic devices such

Received: February 10, 2015
Accepted: April 3, 2015
Published: April 3, 2015

DOI: 10.1021/acsami.5b01327
ACS Appl. Mater. Interfaces 2015, 7, 8789−8797

as touch screens, OLEDs, organic photodiodes, and organic solar cells could be fabricated on flexible CNT electrodes deposited on PET or PEN substrates.

However, the application of CNT films as electrodes in organic electronics is still challenging because of the surface roughness of the CNT films, which is much higher than that of ITO films. The mainly encountered problem with e.g. OPV devices buildup on CNT electrodes, results from CNTs, which could penetrate the active layer.[29] Such CNTs would result in a short cut of the solar cell. A similar investigation has been reported by Leem et al., in which the silver nanowire as the lower electrode shows spike heights exceeding 100 nm. Unless adequately buffered by a suitable coating, the devices are likely to short through subsequent layers, thus hindering the device operation.[30] In addition, a large surface roughness of the CNTs could also disrupt the continuous distribution of the organic bulk heterojunction morphology and prevent uniform hole collection at the CNT surface. To address these problems, a decrease of the surface roughness is required. One potential way of achieving a reduced surface roughness is to add a blocking layer, which is typically used in the OPV device architecture. For instance, a blocking layer of PEDOT:PSS is frequently used.[23,31,32] An aqueous PEDOT:PSS solution can be coated on top of the CNT layer to smooth the surface morphology of the CNT film and to avoid local shunts.

For deposition of a PEDOT:PSS layer on top of the bottom electrode, spin coating is the commonly used method.[33,34] However, as shown previously, CNT films are difficult to wet by polar liquids and water.[35] The CNT films have a high surface roughness and a low surface energy, both contributing to the hydrophobic nature of the CNT films.[36] In general, it is reported that oxygen plasma treatment is an effective way to alter the surface energy and also clean a film surface.[37−39] Oxygen plasma treatment is normally used in the treatment of ITO electrodes to improve the wetting properties before deposition of an aqueous PEDOT:PSS solution.[40,41] However, oxygen plasma treatment is not suitable for CNT electrodes because the CNT film could be oxidized during the oxygen plasma treatment even at very short exposure time, which sacrifices the conductivity or even completely destroys the CNT films.[42,43] Therefore, in order to improve the wetting of the CNT film surface, an alternative process to the oxygen plasma treatment is required, which guarantees the formation of a fully covered PEDOT:PSS layer as well as a good contact between the PEDOT:PSS layer and CNT electrodes.

A general method of depositing a PEDOT:PSS layer on top of a CNT surface is described in the literature via the addition of some solvent additives to the PEDOT:PSS solution before spin coating.[35] For example, different amounts of methanol have been added to PEDOT:PSS to enable spin coating, however, without clarifying the conditions for an optimum electrode performance. To the best of our knowledge, there is no detailed investigation focusing on understanding such optimum conditions. Moreover, fundamental knowledge on how methanol changes the performance of the PEDOT:PSS layer on top of the CNT films on flexible substrates is still limited.

In the present investigation, we address different deposition conditions of aqueous PEDOT:PSS solutions on top of the CNT films on flexible PET substrates. Our aim is to fabricate a buffer layer of PEDOT:PSS on CNT/PET substrates with a transmission behavior in the ultraviolet/visible (UV/vis) region similar to that of the original CNT/PET substrates. Additionally, a higher conductivity of the PEDOT:PSS/CNT layers is also desirable, which however might not be important for PEDOT:PSS layers deposited on flat electrodes such as ITO with the function of a blocking layer in organic solar cells. With the improvement of the wettability of the CNTs, the PEDOT:PSS layer can diffuse into the CNT network and good conductivity will be attributed to good contact at the interface between the CNTs and PEDOT:PSS layer. Accordingly, it is beneficial for charge extraction or injection at such electrodes. Moreover, the CNT/PET substrates, which are used in the present investigation, are already a commercial product, which is potentially cheap, easy to buy, and available in large quantity. In detail, different PEDOT:PSS films on top of CNT/PET substrates, deposited from an aqueous PEDOT:PSS solution with different volume fractions of methanol, are examined. The film thicknesses of all samples are probed with X-ray reflectivity (XRR) measurements, and the optical properties of all samples are determined by UV/vis absorption spectroscopy. Atomic force microscopy (AFM) measurements reveal the resulting surface morphology and surface roughness of the PEDOT:PSS films on top of the CNT/PET substrates for different volume fractions of methanol. In addition, the inner morphology of the PEDOT:PSS films on top of the CNT/PET substrates are probed with grazing-incidence small-angle X-ray scattering (GISAXS) for different volume fractions of methanol. This requires that the scattering technique GISAXS, which is so far only applied to rigid substrates, is successfully extended to the investigation of flexible substrates for the first time.

2. EXPERIMENTAL SECTION

2.1. Materials. The PEDOT:PSS solution used in this investigation was obtained from Sigma-Aldrich, with a PEDOT content of 0.5 wt % and a PSS content of 0.8 wt % in the aqueous dispersion. The commercial CNT/PET substrates were purchased from Unidym (Sunnyvale, CA) and specified with a maximum sheet resistance of 225 Ω/sq and a minimum transmission of 73%. As described by the company, the CNT films were deposited from a water-based double-wall CNT solution using a sodium dodecyl sulfate derivate as the dispersant via a roll-to-roll compatible process on PET. The PET foil was semicrystalline.

2.2. Sample Preparation. The PEDOT:PSS solution as obtained was kept in an ultrasonic bath for 15 min and then filtered with a poly(vinylidene difluoride) filter (0.45 μm). Methanol was added to the PEDOT:PSS solution with different volume fractions of 0, 33, 50, 67, and 75 vol %. The PEDOT:PSS solutions with different amounts of methanol were spin-coated on precleaned CNT/PET substrates after stirring for 15 min at room temperature. In order to control the PEDOT:PSS film thickness, the spin-coating parameters were optimized as shown in Table 1. Only in the case of 75 vol % methanol no larger film thickness was achieved because of the low viscosity of the solution. After spin coating, all PEDOT:PSS films on CNT/PET substrates were directly annealed at 120 °C for 2 h to evaporate residual solvents from the films.

2.3. Measurements. *2.3.1. Resistivity.* In order to investigate the conductivity of the PEDOT:PSS layers on top of CNT/PET substrates, the resistivity values were derived from the resistance measurements of all samples in horizontal and perpendicular directions, as illustrated in Figure 1.[44]

2.3.2. AFM. The surface structures were probed by using an AFM instrument (Jeol JSPM 5200) with point-probe silicon SPM sensors, type CSC 12/AIBS/50 from μMash operating in tapping mode. The resonance frequency of the cantilever was set to 135 kHz. The original data were analyzed with the analysis software *WinSPM Processing Software*.

DOI: 10.1021/acsami.5b01327
ACS Appl. Mater. Interfaces 2015, 7, 8789−8797

Table 1. Parameters for Spin Coating of a PEDOT:PSS Solution with Different Volume Fractions of Methanol as Chosen in the Present Investigation and Resulting Film Thicknesses

	volume fraction of methanol (vol %)				
	0	33	50	67	75
rotational speed (rpm)	3000	2500	2000	600	600
				2500	1500
spinning time (s)	60	60	60	60	60
				60	60
film thickness (nm)	83 ± 1	87 ± 1	81 ± 1	83 ± 1	50 ± 1

2.3.3. UV/Vis Spectroscopy. Transmission measurements were performed with a UV/vis spectrometer Lambda 35 (PerkinElmer) using a wavelength range from 190 to 1100 nm. The measurements were carried out with a scan rate of 120 nm/min and a slit width of 2 nm.

2.3.4. XRR. The XRR experiments were performed with a Siemens D 5000 diffractometer using a $\theta - 2\theta$ geometry, an X-ray wavelength of 0.154 nm, and a 2θ range from 0.02° to 6.50°. The XRR data were fitted with the software *Parratt32*, which is based on the Parratt algorithm.[45] The resulting film-thickness values of the PEDOT:PSS films are shown in Table 1. The film thickness of the CNT films was 44 nm.

2.3.5. GISAXS. The GISAXS experiments were carried out at the synchrotron beamline BW4 at the DORIS III storage ring at HASYLAB, DESY, Hamburg, Germany.[46] The wavelength of the X-ray beam was 0.1381 nm, and the sample detector distance was 2.14 m. Because of challenges in the alignment of flexible PET substrates, the incident angles used in the investigation covered a range from 0.27° to 0.44°. The two-dimensional (2D) GISAXS data were recorded with a MarCCD 165 detector, with 2048 × 2048 pixels and a pixel size of 79.1 × 79.1 μm^2. The signals of the direct beam and the specular peak were shielded by two round beam stops to avoid oversaturation of the detector. For analysis of the GISAXS data, horizontal line cuts at the critical angle of PEDOT:PSS and vertical line cuts at $q_y = 0$ were taken and analyzed, respectively.[47] The horizontal line cuts were fitted with a model based on the effective surface approximation model.

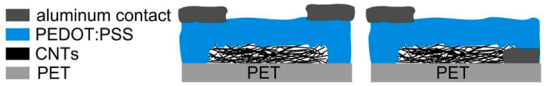

Figure 1. Sketch of resistance measurements in horizontal (left) and perpendicular (right) directions, respectively.

3. RESULTS AND DISCUSSION

3.1. Optical Properties. The optical performance of all layers underneath the active layer is quite important for organic electronic devices such as, for example, OPV devices in order to get high absorption of the active layer because high absorption of the active layer directly improves the efficiency of the solar cell. Therefore, it is critical to keep the transmission of the PEDOT:PSS layer on top of the CNT/PET substrates as high as possible. To investigate how the addition of methanol affects the optical properties, the transmission is measured in the UV/vis region. The bare CNT/PET substrate, a PEDOT:PSS layer without the addition of methanol on top of CNT/PET substrates (named pure in the following), and PEDOT:PSS films on top of CNT/PET substrates prepared with different volume fractions of methanol are probed with UV/vis spectroscopy. Figure 2 shows the transmission spectra of all samples. For all PEDOT:PSS films on top of the CNT/PET substrates, the transmission is decreased, irrespective of deposition from the aqueous PEDOT:PSS solutions without or with methanol. This decrease originates from absorption of

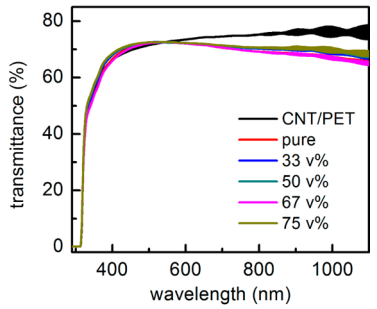

Figure 2. Transmission spectra of the bare CNT/PET substrate, pure PEDOT:PSS layers on top of CNT/PET substrates, and PEDOT:PSS films on top of CNT/PET substrates with volume fractions of methanol of 33, 50, 67, and 75 vol %, as indicated in the inset.

the PEDOT:PSS layer. However, in all cases, this decrease is still so limited that it does not prevent application in organic electronic devices such as organic solar cells. The changes in the intensity of the transmission spectra among different PEDOT:PSS films on top of the CNT/PET substrates can be attributed to different film thicknesses, as shown in Table 1. Besides, all of the spectra show oscillations of the transmittance (from 750 to 1100 nm) due to the Fabry-Pérot interference fringes originating from interface between the thin layers of CNT film and PET substrates.[48] We also observe this phenomenon in the UV/vis measurement of ITO on a PET substrate. In addition, the spectra exhibit no shift in wavelength between those of the pure PEDOT:PSS layer and those with methanol. Therefore, it is inferred that methanol does not change the properties of PEDOT:PSS. Consequently, adding methanol to an aqueous PEDOT:PSS solution has a minor effect on the optical properties (transmission) of the PEDOT:PSS layer, and regarding the transmission, no preferential amount of methanol addition can be identified.

3.2. Conductivity. The selected CNT/PET substrates show a reasonable conductivity, as presented in Figure 3. With respect to application in organic electronics, the conductivity of PEDOT:PSS placed on top of CNT/PET substrates is also quite important because a higher conductivity of the PEDOT:PSS layer provides a lower series resistance. The resistivities of bare CNT/PET substrates, pure PEDOT:PSS films on top of the CNT/PET substrates, and PEDOT:PSS films on top of CNT/PET substrates prepared with different volume fractions of methanol (33, 50, 67, and 75 vol %) are compared. The resistivity values are derived from the resistance measurements, which are carried out in two directions, perpendicular and horizontal to the sample surfaces, respectively.[44] The resulting resistivity values in both directions are shown in Figure 3. Focusing on the results obtained from the measurements in the perpendicular direction, the CNT/PET substrate shows the lowest resistivity of all samples. In the

DOI: 10.1021/acsami.5b01327
ACS Appl. Mater. Interfaces 2015, 7, 8789−8797

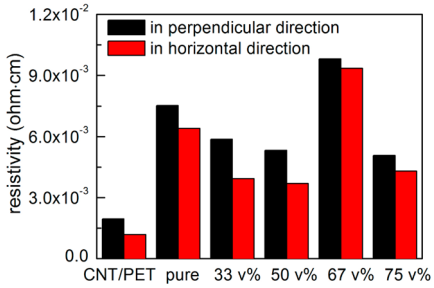

Figure 3. Resistivity of the bare CNT/PET substrate, pure PEDOT:PSS film on top of CNT/PET substrates, and PEDOT:PSS films on top of CNT/PET substrates with volume fractions of methanol 33, 50, 67, and 75 vol %.

case of the pure PEDOT:PSS solution deposited on top of CNT/PET substrates, the resistivity almost increases by 4 times compared to that of the bare CNT/PET substrate. Using PEDOT:PSS solutions with 33, 50, and 75 vol % methanol results in a reduced resistivity by more than 1.65×10^{-3} Ω·cm compared to that of the pure PEDOT:PSS sample, while for the sample with 67 vol % methanol, the resistivity is strongly increased again. In the case of the sample with 75 vol % methanol, the resistivity is decreased again because of the thinner PEDOT:PSS layer, which implies that, in general, lower values can be achieved for lower PEDOT:PSS layer thicknesses. With respect to the resistivity in the horizontal direction, a trend very similar to that for the perpendicular direction is observed. However, the resistivity values derived in horizontal measurements are lower than those measured in the perpendicular direction because the CNTs are lying predominantly on the PET surface, which gives better conductivity in the horizontal direction. In the case of the PEDOT:PSS layer, it is known from the literature that the main PEDOT-rich clusters are separated by lamellae of PSS.[49] If oriented parallel to the surface of the PEDOT:PSS layer, this will also contribute to the better conductivity in the parallel direction compared to that in the perpendicular direction.[49] Anyhow, the stack of a PEDOT:PSS layer on top of CNT/PET substrates shows better conductivity in the parallel direction than in the perpendicular direction, which is favorable for collecting free charge carriers as an electrode. With respect to the lowest resistivity, the PEDOT:PSS layer with 50 vol % methanol is the optimum case for deposition on top of CNT/PET substrates. In order to correlate this property with the structure in the PEDOT:PSS layer on top of CNT/PET substrates, the morphology is investigated.

3.3. Surface Morphology. The surface morphology of the samples is probed with AFM measurements, and selected topographic images are shown in Figure 4. The presence of the PEDOT:PSS layer results in the desired smoothing of the surface structures. With the addition of methanol to the PEDOT:PSS solution, the surface features get more pronounced. To visualize this tendency, selected line cuts from the

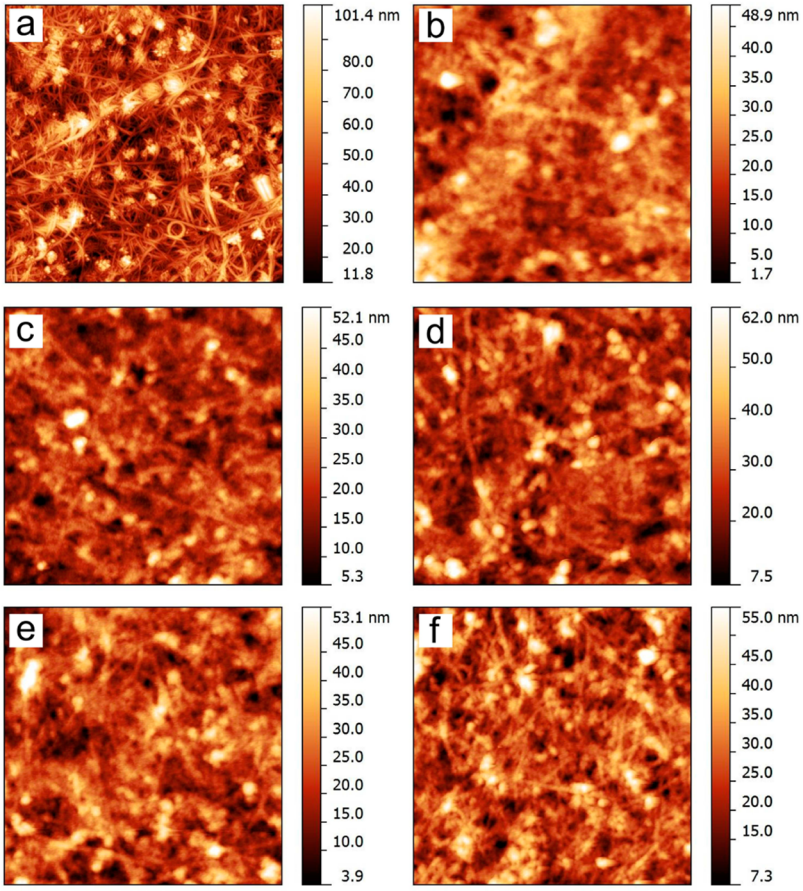

Figure 4. AFM images (4×4 μm^2) showing the topography of the (a) bare CNT/PET substrate, (b) pure PEDOT:PSS layer on top of CNT/PET substrate, and PEDOT:PSS films on top of CNT/PET substrates prepared with volume fractions of methanol of (c) 33, (d) 50, (e) 67, and (f) 75 vol %.

DOI: 10.1021/acsami.5b01327
ACS Appl. Mater. Interfaces 2015, 7, 8789−8797

AFM data are shown in Figure 5a and the root-mean-square (rms) surface roughness is extracted from the AFM data (see Figure 5b). As presented in Figure 4a, it is obvious that CNTs are physically cross-linked and bundled together, resulting in the high conductivity of the CNT film. At the same time, the topography of the bare CNT/PET substrate exhibits a large surface roughness (rms value of 13 nm). As discussed in the Introduction, if the CNT/PET substrates with such high surface roughness are used in organic electronics, some CNTs can penetrate the active layer placed on top of the CNT film, which could result in a short cut of the devices. Figure 5b shows that the surface roughness can be decreased by nearly 50% compared to the bare CNT/PET substrate after deposition of PEDOT:PSS films on top of CNT/PET substrates. The PEDOT:PSS layers reduce the surface roughness compared to the bare CNT/PET substrates, independent of the volume fraction of methanol. However, with increasing volume fraction of methanol in the PEDOT:PSS aqueous solution, the surface roughness of the PEDOT:PSS layers increases again.

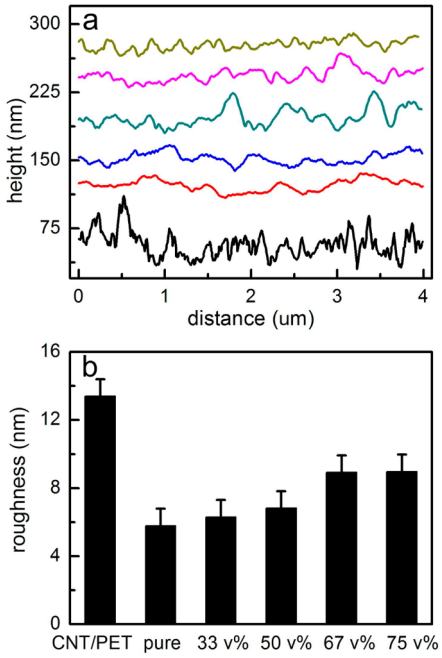

Figure 5. (a) Selected cross sections of the AFM topography data and (b) rms surface roughness extracted from the AFM data in the case of the bare CNT/PET substrate, pure PEDOT:PSS layer on top of CNT/PET substrate, and PEDOT:PSS films on top of CNT/PET substrates with 33, 50, 67, and 75 vol % methanol. They are shown from the bottom to the top and shifted along the *y* axis for clarity in part a.

In the case where PEDOT:PSS layers are deposited on top of CNT/PET substrates, without or with methanol, these PEDOT:PSS layers follow the surface morphology of CNT/PET substrates underneath (see Figure 4). With increasing volume fraction of methanol in the PEDOT:PSS aqueous solution, the PEDOT:PSS layers better replicate the surface features of the CNT surfaces, which explains why adding more methanol induces higher surface roughness values. In the cross-sectional data (Figure 5a), the bare CNT/PET surface shows sharp and small structures. When pure PEDOT:PSS is deposited on top, these surface features are smoothed and the small structures are merged into large domains. With the addition of methanol to the PEDOT:PSS solution, the surface features become rougher compared to the pure PEDOT:PSS layer, and both small and big structures show up. In the case when a large amount of methanol is added to the PEDOT:PSS solution, the PEDOT:PSS surface shows quite similar structures, as seen from the bare CNT/PET substrate. In addition, on a larger scale, the PEDOT:PSS coating with 75 vol % methanol appears to be heterogeneous.

The reason for the change in the morphology of the PEDOT:PSS layer as a function of the amount of methanol is an improved wetting and a lower viscosity. The improved wetting of the CNT/PET substrate results in a better contact between the PEDOT:PSS and CNT/PET substrates. In organic solar cells, such good contact between the CNT/PET and PEDOT:PSS films gives rise to a low series resistance, which, in turn, will result in a higher power conversion efficiency. On the basis of these findings, it is expected that a PEDOT:PSS layer deposited from a PEDOT:PSS aqueous solution with some volume fraction of methanol is better suited compared to a pure PEDOT:PSS solution if CNT/PET substrates are used in organic electronics.

Better contact between the PEDOT:PSS layer and CNT/PET substrate seems also to be the reason for an increase of the conductivity. However, the observed surface morphologies cannot fully explain the changes in the conductivity of the samples. Hence, in addition to the surface morphology, the inner structure needs to be considered as well.

3.4. Inner Film Morphology. To investigate the inner morphology, GISAXS measurements are performed. GISAXS measurements give the average information about the inner morphology of the sample on a mesoscopic scale.[47,50−54] Commonly, GISAXS measurements are only performed on solid substrates.[55,56] To the best of our knowledge, in the present work GISAXS measurements on flexible substrates are carried out for the first time. Because of the flexibility of the CNT/PET substrate, alignment of the sample in the X-ray beam is more difficult compared to that of rigid substrates such as silicon or glass. In order to solve this problem, the samples are fixed on a silicon substrate with the help of surface tension from a water layer. The 2D GISAXS data of the bare CNT/PET substrate (Figure 6a), the pure PEDOT:PSS layer on top of CNT/PET substrates (Figure 6b), and the PEDOT:PSS films with different volume fractions of methanol on top of CNT/PET substrates (Figure 6c−f) show characteristic scattering features. In all 2D GISAXS data (Figure 6), the material-specific Yoneda peak is observed at the position of the critical angles.[47,53,57−60] In the case of the bare CNT/PET substrate (Figure 6a), the Yoneda peak has a different position compared to that of the PEDOT:PSS covered samples (Figure 6b−f) because the Yoneda peak of PEDOT:PSS dominates.

Two well-pronounced side maxima are seen in the 2D GISAXS data of the bare CNT/PET sample. These two side maxima arise from a lateral nanostructure in the CNT layer. Rueda et al. revealed similar dominant features in the 2D GISAXS data of the nanostructured grating samples.[59] However, in contrast to an anisotropic grating structure, the CNTs have no preferential orientation and an isotropic GISAXS pattern results. This is consistent with the AFM measurements (Figure 4a), showing a random network of CNTs. When the pure PEDOT:PSS layer is deposited on top of CNT/PET substrates, these side maxima disappear (Figure 6b), whereas for the PEDOT:PSS films with different volume fractions of methanol, the two side maxima remain present.

DOI: 10.1021/acsami.5b01327
ACS Appl. Mater. Interfaces 2015, 7, 8789−8797

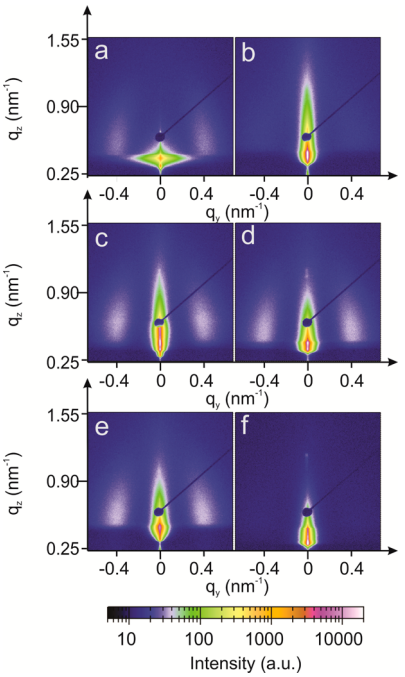

Figure 6. 2D GISAXS data of the (a) bare CNT/PET substrate, (b) pure PEDOT:PSS layer on top of CNT/PET substrate, and PEDOT:PSS films with different volume fractions of methanol: (c) 33, (d) 50, (e) 67, and (f) 75 vol %. The color code represents the scattering intensity as indicated. The specular peak is shielded by a beam stop.

Only for the highest amount of methanol (75 vol %) in the PEDOT:PSS aqueous solution are the side maxima are not found.

To extract quantitative information from the 2D GISAXS data, horizontal line cuts are analyzed, as presented in Figure 7. These line cuts show the absence or presence of the side maxima as well. The line cuts are fitted with a model based on the effective surface approximation within the distorted-wave Born approximation, assuming two characteristic lateral

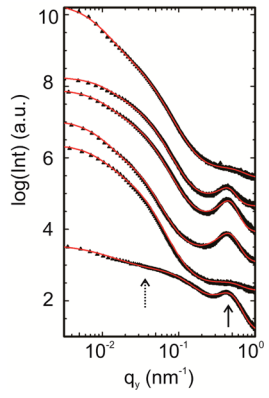

Figure 7. Horizontal line cuts of the 2D GIAXS data (symbols) shown together with the model fits (lines). From bottom to top data of the bare CNT/PET substrate, pure PEDOT:PSS layer on top of CNT/PET substrate, and PEDOT:PSS films with volume fractions of methanol of 33, 50, 67, and 75 vol % are shown. The curves are shifted along the y axis for clarity. The positions of characteristic structures with sizes of 14.2 ± 0.5 nm (arrow) and 175 ± 25 nm (dotted arrow) for CNT/PET are indicated.

structures with a Lorentzian distribution function as well as taking the resolution function into account.[2]

The structure sizes determined from the fitting are plotted in Figure 8a. For the bare CNT/PET substrate, the two

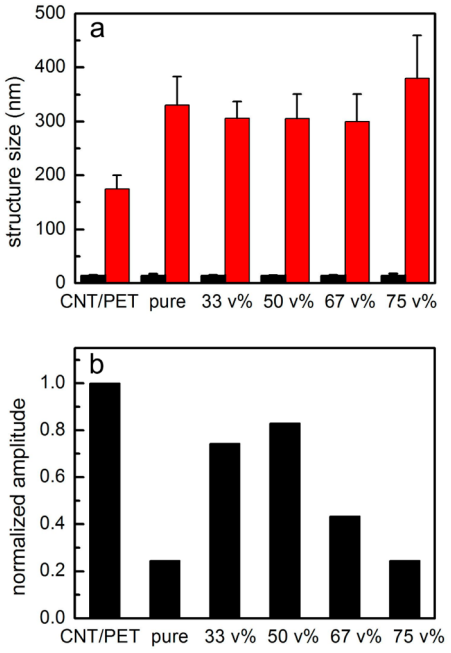

Figure 8. (a) Characteristic structure sizes extracted from the fits of the horizontal line cuts. (b) Amplitude of the side maximum in the horizontal line cut related to the small-sized structure. All amplitudes are normalized to that of the CNT/PET substrate sample.

characteristic structures are 14.2 ± 0.5 and 175 ± 25 nm, indicated with two arrows in Figure 7. The small-sized structure of 14 nm is assigned to the two maxima arising in the 2D GISAXS data, as shown in Figure 6a, which is also observed in all other films irrespective what amount of methanol has been added to PEDOT:PSS. Thus, we assign this small-sized structure to the average size of CNT bundles. In contrast, the large-sized structure of 175 nm, observed in the case of the bare CNT/PET sample, is not found in the samples overcoated with PEDOT:PSS. Instead, for the samples with a PEDOT:PSS layer, a structure larger than 300 nm is present. This larger structure is related to the polymer layer.

In addition to the discussion about lateral structures extracted from the peak position in the horizontal line cuts, the amplitude of the side maxima can be addressed (see Figure 7). Whereas all horizontal line cuts exhibit a peak at a very similar q_y position, the amplitudes of these peaks are quite different from one to another. To visualize these differences in amplitudes, normalized values are shown in Figure 8b. In the case of the bare CNT/PET sample, the highest intensity is observed compared to those of the other samples because structures in the CNT layer on top of the PET foil are probed directly and no overlayer is present. The pure PEDOT:PSS film on top of CNT/PET substrates shows the lowest normalized value because the pure PEDOT:PSS layer cannot follow the details in the morphology of the CNT layer underneath, which is caused by the bad contact between the CNT/PET surface and PEDOT:PSS layers. With the addition of methanol, this contact is improved, and the amplitude is enlarged up to a volume fraction of 50 vol % methanol. For higher amounts of

DOI: 10.1021/acsami.5b01327
ACS Appl. Mater. Interfaces 2015, 7, 8789−8797

methanol added, the values of the normalized amplitudes decrease again. Thus, in the normalized amplitudes, we observe a trend very similar to that of the resistivity except for the highest amount of added methanol because of the different PEDOT:PSS film thicknesses (see Figure 3). High amplitudes occur for samples that exhibit low resistivity.

Figure 9 summarizes in a schematic way how methanol addition affects the morphology of the PEDOT:PSS layers on top of CNT/PET substrates. The sketches show the cross section of the samples. The blue parts represent the PEDOT:PSS layers, and the black lines represent the CNTs. The PET foil is not displayed. As depicted in Figure 9a, the pure PEDOT:PSS layer has poor contact with the CNTs because of the poor wettability and high surface roughness of the CNTs. From nonwetted parts, air cushions result, which strongly contribute to the scattering and thereby reduce the contributions from the CNT/PET substrates. When using a moderate amount of methanol (Figure 9b), the wettability of the CNTs is strongly improved, and a good contact between the PEDOT:PSS layer and CNTs is achieved. In the GISAXS data, the strong scattering contribution from the CNTs goes up again. In the case of the addition of a larger amount of methanol, the PEDOT:PSS layers are no longer continuous and homogeneous (Figure 9c). In the GISAXS data, the contribution of the CNT nanostructure is weakened. When the highest amount of methanol is added to the PEDOT:PSS solution (Figure 9d), the PEDOT:PSS layer has a smaller thickness because it permeates into the CNTs. This introduces a grainy film morphology. Thus, novel and less regular nanostructures are generated, which cause the absence of well-pronounced peaks in the GISAXS data.

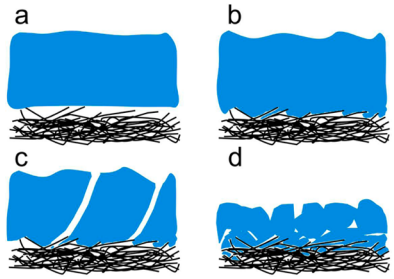

Figure 9. Schematic morphology of the PEDOT:PSS layers (blue) on top of CNTs (black lines) without showing the PET foil underneath: (a) pure PEDOT:PSS layer showing poor contact with CNTs; (b) PEDOT:PSS layer with a moderate methanol amount, which improves the wettability of CNTs and, accordingly, a good contact with the CNTs is achieved; (c) discontinuous PEDOT:PSS layer on top of CNTs due to the addition of a large amount methanol. With the largest amount of methanol, the PEDOT:PSS film has a smaller thickness because it permeates into CNTs and exhibits grains, as shown in part d.

The changes in the conductivity are also explained from this morphology development. The highest conductivity is found for the bare CNT films because that of PEDOT:PSS is intrinsically lower, and air gaps between the PEDOT:PSS layer and CNTs increase the resistivity of whole parts of the film. By doping with methanol, the conductivity can be improved in case the contact between the CNTs and PEDOT:PSS layer is best. When a moderate amount of methanol is added, an optimized contact facilitates charge transport between PEDOT:PSS and the CNTs. Therefore, a reduced resistivity is achieved. However, excessive use of methanol breaks the continuous PEDOT:PSS layer, which increases the resistivity in the PEDOT:PSS layer. The conductivity of the whole system is decreased. When the highest amount of methanol is added, the conductivity recovered slightly because of the reduced film thickness of the PEDOT:PSS layer, which has itself a lower conductivity compared to that of the CNTs.

4. CONCLUSION

In summary, adding methanol in PEDOT:PSS aqueous solutions improves the wetting of PEDOT:PSS on CNT/PET substrates. At the same time, the methanol addition also recovers the conductivity of PEDOT:PSS on top of CNT/PET. To clarify the reason for the recovery of the conductivity, the transmission data, the surface morphologies, and the inner morphologies are discussed for different amounts of methanol added and compared to those of the uncoated CNT/PET samples. An amount of 50 vol % methanol being added into the PEDOT:PSS solution is found to be the optimal value for achieving the lowest resistivity in both the perpendicular and horizontal directions, which is only moderately larger than that of the bare CNT/PET samples. Because these PEDOT:PSS films on top of the CNT/PET show significantly smaller surface roughness values compared to those of the bare CNT/PET substrates, such a combination appears to be very promising for potential use in organic electronic devices, e.g., in organic solar cells, OLEDs, or organic photodiodes. In particular, in organic solar cells using the normal device architecture, the CNT would resemble the bottom electrode and the PEDOT:PSS film the commonly used blocking layer, which intrinsically does not need to have a high conductivity.

AUTHOR INFORMATION

Corresponding Author

*E-mail: muellerb@ph.tum.de. Tel: +49 (0)89 289 12451. Fax: +49 (0)89 289 12473.

Author Contributions

All authors have given approval to the final version of the manuscript.

Notes

The authors declare no competing financial interest.

ACKNOWLEDGMENTS

Financial support by TUM Solar in the frame of the Bavarian Collaborative Research Project “Solar technologies go Hybrid” (SolTec), by the GreenTech Initiative (Interface Science for Photovoltaics) of the EuroTech Universities, and by the Nanosystems Initiative Munich is acknowledged. W.W. thanks the China Scholarship Council and E.M.H. the Munich School of Engineering for funding. We thank B. Balzer and T. Hugel for the possibility of performing AFM measurements. We thank D. Magerl for implementing the fitting model.

REFERENCES

(1) Kim, J. Y.; Lee, K.; Coates, N. E.; Moses, D.; Nguyen, T.-Q.; Dante, M.; Heeger, A. J. Efficient Tandem Polymer Solar Cells Fabricated by All-Solution Processing. *Science* **2007**, *317*, 222−225.

(2) Ruderer, M. A.; Guo, S.; Meier, R.; Chiang, H.-Y.; Körstgens, V.; Wiedersich, J.; Perlich, J.; Roth, S. V.; Müller-Buschbaum, P. Solvent-Induced Morphology in Polymer-Based Systems for Organic Photovoltaics. *Adv. Funct. Mater.* **2011**, *21*, 3382−3391.

DOI: 10.1021/acsami.5b01327
ACS Appl. Mater. Interfaces 2015, 7, 8789−8797

(3) Ruderer, M. A.; Müller-Buschbaum, P. Morphology of Polymer-Based Bulk Heterojunction Films for Organic Photovoltaics. *Soft Matter* **2011**, *7*, 5482−5493.
(4) Liang, Y.; Xu, Z.; Xia, J.; Tsai, S.-T.; Wu, Y.; Li, G.; Ray, C.; Yu, L. For the Bright Future—Bulk Heterojunction Polymer Solar Cells with Power Conversion Efficiency of 7.4%. *Adv. Mater.* **2010**, *22*, E135−E138.
(5) Coakley, K. M.; McGehee, M. D. Conjugated Polymer Photovoltaic Cells. *Chem. Mater.* **2004**, *16*, 4533−4542.
(6) Li, G.; Shrotriya, V.; Huang, J.; Yao, Y.; Moriarty, T.; Emery, K.; Yang, Y. High-Efficiency Solution Processable Polymer Photovoltaic Cells by Self-Organization of Polymer Blends. *Nat. Mater.* **2005**, *4*, 864−868.
(7) Erb, T.; Zhokhavets, U.; Gobsch, G.; Raleva, S.; Stühn, B.; Schilinsky, P.; Waldauf, C.; Brabec, C. J. Correlation Between Structural and Optical Properties of Composite Polymer/Fullerene Films for Organic Solar Cells. *Adv. Funct. Mater.* **2005**, *15*, 1193−1196.
(8) Kim, Y.; Cook, S.; Tuladhar, S. M.; Choulis, S. A.; Nelson, J.; Durrant, J. R.; Bradley, D. D. C.; Giles, M.; McCulloch, I.; Ha, C. S.; Ree, M. A strong regioregularity effect in self-organizing conjugated polymer films and high-efficiency polythiophene:fullerene solar cells. *Nat. Mater.* **2006**, *5*, 197−203.
(9) Nguyen, L. H.; Hoppe, H.; Erb, T.; Günes, S.; Gobsch, G.; Sariciftci, N. S. Effects of Annealing on the Nanomorphology and Performance of Poly(alkylthiophene):Fullerene Bulk-Heterojunction Solar Cells. *Adv. Funct. Mater.* **2007**, *17*, 1071−1078.
(10) Green, M. A.; Emery, K.; Hishikawa, Y.; Warta, W.; Dunlop, E. D. Solar Cell Efficiency Tables (Version 44). *Prog. Photovoltaics* **2014**, *22*, 701−710.
(11) You, J.; Dou, L.; Yoshimura, K.; Kato, T.; Ohya, K.; Moriarty, T.; Emery, K.; Chen, C.-C.; Gao, J.; Yang, Y. A Polymer Tandem Solar Cell with 10.6% Power Conversion Efficiency. *Nat. Commun.* **2013**, *4*, 1446.
(12) Zawacka, N. K.; Andersen, T. R.; Andreasen, J. W.; Rossander, L. H.; Dam, H. F.; Jørgensen, M.; Krebs, F. C. The Influence of Additives on the Morphology and Stability of Roll-to-Roll Processed Polymer Solar Cells Studied through ex situ and in situ X-ray Scattering. *J. Mater. Chem. A* **2014**, *2*, 18644−18654.
(13) Burgués-Ceballos, I.; Stella, M.; Lacharmoise, P.; Martínez-Ferrero, E. Towards Industrialization of Polymer Solar Cells: Material Processing for Upscaling. *J. Mater. Chem. A* **2014**, *2*, 17711−17722.
(14) Li, N.; Baran, D.; Spyropoulos, G. D.; Zhang, H.; Berny, S.; Turbiez, M.; Ameri, T.; Krebs, F. C.; Brabec, C. J. Environmentally Printing Efficient Organic Tandem Solar Cells with High Fill Factors: A Guideline towards 20% Power Conversion Efficiency. *Adv. Energy. Mater.* **2014**, *4*, 1400084.
(15) Ou, E. C.-W.; Hu, L.; Raymond, G. C. R.; Soo, O. K.; Pan, J.; Zheng, Z.; Park, Y.; Hecht, D.; Irvin, G.; Drzaic, P.; Gruner, G. Surface-Modified Nanotube Anodes for High Performance Organic Light-Emitting Diode. *ACS Nano* **2009**, *3*, 2258−2264.
(16) Kawai, T.; Maekawa, Y.; Kusabiraki, M. Plasma Treatment of ITO Surfaces to Improve Luminescence Characteristics of Organic Light-Emitting Devices with Dopants. *Surf. Sci.* **2007**, *601*, 5276−5279.
(17) Lu, H.-T.; Yokoyama, M. Plasma Preparation on Indium−Tin-Oxide Anode Surface for Organic Light Emitting Diodes. *J. Cryst. Growth* **2004**, *260*, 186−190.
(18) Cairns, D. R.; Crawford, G. P. Electromechanical Properties of Transparent Conducting Substrates for Flexible Electronic Displays. *Proc. IEEE* **2005**, *93*, 1451−1458.
(19) Wang, Y.; Liu, S.; Dang, F.; Li, Y.; Yin, Y.; Liu, J.; Xu, K.; Piao, X.; Xie, W. An Efficient Flexible White Organic Light-Emitting Device with a Screen-Printed Conducting Polymer Anode. *J. Phys. D: Appl. Phys.* **2012**, *45*, 402002.
(20) Saran, N.; Parikh, K.; Suh, D.-S.; Muñoz, E.; Kolla, H.; Manohar, S. K. Fabrication and Characterization of Thin Films of Single-Walled Carbon Nanotube Bundles on Flexible Plastic Substrates. *J. Am. Chem. Soc.* **2004**, *126*, 4462−4463.
(21) Li, J.; Hu, L.; Liu, J.; Wang, L.; Marks, T. J.; Grüner, G. Indium Tin Oxide Modified Transparent Nanotube Thin Films as Effective Anodes for Flexible Organic Light-Emitting Diodes. *Appl. Phys. Lett.* **2008**, *93*, 083306.
(22) Huang, J.; Miller, P. F.; Wilson, J. S.; de Mello, A. J.; de Mello, J. C.; Bradley, D. D. C. Investigation of the Effects of Doping and Post-Deposition Treatments on the Conductivity, Morphology, and Work Function of Poly(3,4-ethylenedioxythiophene)/poly(styrenesulfonate) Films. *Adv. Funct. Mater.* **2005**, *15*, 290−296.
(23) Fehse, K.; Walzer, K.; Leo, K.; Lövenich, W.; Elschner, A. Highly Conductive Polymer Anodes as Replacements for Inorganic Materials in High-Efficiency Organic Light-Emitting Diodes. *Adv. Mater.* **2007**, *19*, 441−444.
(24) Tyler, T. P.; Brock, R. E.; Karmel, H. J.; Marks, T. J.; Hersam, M. C. Electronically Monodisperse Single-Walled Carbon Nanotube Thin Films as Transparent Conducting Anodes in Organic Photovoltaic Devices. *Adv. Energy. Mater.* **2011**, *1*, 785−791.
(25) Balamurugan, J.; Pandurangan, A.; Kim, N. H.; Lee, J. H. Facile Synthesis of High Quality Multi-Walled Carbon Nanotubes on Novel 3D KIT-6: Application in High Performance Dye-Sensitized Solar Cells. *Nanoscale* **2014**, *7*, 679−689.
(26) Li, Z.; Kulkarni, S. A.; Boix, P. P.; Shi, E.; Cao, A.; Fu, K.; Batabyal, S. K.; Zhang, J.; Xiong, Q.; Wong, L. H.; Mathews, N.; Mhaisalkar, S. G. Laminated Carbon Nanotube Networks for Metal Electrode-Free Efficient Perovskite Solar Cells. *ACS Nano* **2014**, *8*, 6797−6804.
(27) Ulbricht, R.; Lee, S. B.; Jiang, X.; Inoue, K.; Zhang, M.; Fang, S.; Baughman, R. H.; Zakhidov, A. A. Transparent Carbon Nanotube Sheets as 3-D Charge Collectors in Organic Solar Cells. *Sol. Energy Mater. Sol. Cells* **2007**, *91*, 416−419.
(28) Zhang, J.; Gao, L.; Sun, J.; Liu, Y.; Wang, Y.; Wang, J. Incorporation of Single-Walled Carbon Nanotubes with PEDOT/PSS in DMSO for the Production of Transparent Conducting Films. *Diamond Relat. Mater.* **2012**, *22*, 82−87.
(29) Kim, S.; Yim, J.; Wang, X.; Bradley, D. D. C.; Lee, S.; DeMello, J. C. Spin-and Spray-Deposited Single-Walled Carbon-Nanotube Electrodes for Organic Solar Cells. *Adv. Funct. Mater.* **2010**, *20*, 2310−2316.
(30) Leem, D.-S.; Edwards, A.; Faist, M.; Nelson, J.; Bradley, D. D. C.; de Mello, J. C. Efficient Organic Solar Cells with Solution-Processed Silver Nanowire Electrodes. *Adv. Mater.* **2011**, *23*, 4371−4375.
(31) Vosgueritchian, M.; Lipomi, D. J.; Bao, Z. Highly Conductive and Transparent PEDOT:PSS Films with a Fluorosurfactant for Stretchable and Flexible Transparent Electrodes. *Adv. Funct. Mater.* **2012**, *22*, 421−428.
(32) Palumbiny, C. M.; Heller, C.; Schaffer, C. J.; Körstgens, V.; Santoro, G.; Roth, S. V.; Müller-Buschbaum, P. Molecular Reorientation and Structural Changes in Cosolvent-Treated Highly Conductive PEDOT:PSS Electrodes for Flexible Indium Tin Oxide-Free Organic Electronics. *J. Phys. Chem. C* **2014**, *118*, 13598−13606.
(33) Guo, S.; Brandt, C.; Andreev, T.; Metwalli, E.; Wang, W.; Perlich, J.; Müller-Buschbaum, P. First Step into Space: Performance and Morphological Evolution of P3HT:PCBM Bulk Heterojunction Solar Cells under AM0 Illumination. *ACS Appl. Mater. Interfaces* **2014**, *6*, 17902−17910.
(34) Guo, S.; Ruderer, M. A.; Rawolle, M.; Körstgens, V.; Birkenstock, C.; Perlich, J.; Müller-Buschbaum, P. Evolution of Lateral Structures during the Functional Stack Build-up of P3HT:PCBM-Based Bulk Heterojunction Solar Cells. *ACS Appl. Mater. Interfaces* **2013**, *5*, 8581−8590.
(35) Mattia, D.; Bau, H. H.; Gogotsi, Y. Wetting of CVD Carbon Films by Polar and Nonpolar Liquids and Implications for Carbon Nanopipes. *Langmuir* **2006**, *22*, 1789−1794.
(36) Sethi, S.; Dhinojwala, A. Superhydrophobic Conductive Carbon Nanotube Coatings for Steel. *Langmuir* **2009**, *25*, 4311−4313.
(37) Kim, J. S.; Granström, M.; Friend, R. H.; Johansson, N.; Salaneck, W. R.; Daik, R.; Feast, W. J.; Cacialli, F. Indium−Tin Oxide Treatments for Single- and Double-Layer Polymeric Light-Emitting Diodes: The Relation Between the Anode Physical, Chemical, and

DOI: 10.1021/acsami.5b01327
ACS Appl. Mater. Interfaces 2015, 7, 8789−8797

Morphological Properties and the Device Performance. *J. Appl. Phys.* **1998**, *84*, 6859−6870.
(38) Kim, J. S.; Friend, R. H.; Cacialli, F. Surface Energy and Polarity of Treated Indium−Tin-Oxide Anodes for Polymer Light-Emitting Diodes Studied by Contact-Angle Measurements. *J. Appl. Phys.* **1999**, *86*, 2774−2778.
(39) Yildirim, E. D.; Pappas, D.; Güçeri, S.; Sun, W. Enhanced Cellular Functions on Polycaprolactone Tissue Scaffolds by O_2 Plasma Surface Modification. *Plasma Process. Polym.* **2011**, *8*, 256−267.
(40) Hains, A. W.; Liu, J.; Martinson, A. B. F.; Irwin, M. D.; Marks, T. J. Anode Interfacial Tuning via Electron-Blocking/Hole-Transport Layers and Indium Tin Oxide Surface Treatment in Bulk-Heterojunction Organic Photovoltaic Cells. *Adv. Funct. Mater.* **2010**, *20*, 595−606.
(41) Kim, J.-S.; Cacialli, F.; Friend, R. Surface Conditioning of Indium−Tin Oxide Anodes for Organic Light-Emitting Diodes. *Thin Solid Films* **2003**, *445*, 358−366.
(42) Martínez, M. T.; Callejas, M. A.; Benito, A. M.; Cochet, M.; Seeger, T.; Ansón, A.; Schreiber, J.; Gordon, C.; Marhic, C.; Chauvet, O.; Fierro, J. L. G.; Maser, W. K. Sensitivity of Single Wall Carbon Nanotubes to Oxidative Processing: Structural Modification, Intercalation and Functionalization. *Carbon* **2003**, *41*, 2247−2256.
(43) Zhang, X.; Lei, L.; Xia, B.; Zhang, Y.; Fu, J. Oxidization of Carbon Nanotubes through Hydroxyl Tadical Induced by Pulsed O_2 Plasma and its Application for O_2 Reduction in Electro-Fenton. *Electrochim. Acta* **2009**, *54*, 2810−2817.
(44) Yeo, J.-S.; Yun, J.-M.; Kim, D.-Y.; Park, S.; Kim, S.-S.; Yoon, M.-H.; Kim, T.-W.; Na, S.-I. Significant Vertical Phase Separation in Solvent-Vapor-Annealed Poly(3,4-ethylenedioxythiophene):Poly-(styrenesulfonate) Composite Films Leading to Better Conductivity and Work Function for High-Performance Indium Tin Oxide-Free Optoelectronics. *ACS Appl. Mater. Interfaces* **2012**, *4*, 2551−2560.
(45) Parratt, L. G. Surface Studies of Solids by Total Reflection of X-Rays. *Phys. Rev.* **1954**, *95*, 359−369.
(46) Roth, S. V.; Döhrmann, R.; Dommach, M.; Kuhlmann, M.; Kröger, I.; Gehrke, R.; Walter, H.; Schroer, C.; Lengeler, B.; Müller-Buschbaum, P. Small-Angle Options of the Upgraded Ultrasmall-Angle X-Ray Scattering Beamline BW4 at HASYLAB. *Rev. Sci. Instrum.* **2006**, *77*, 085106.
(47) Müller-Buschbaum, P. Grazing Incidence Small-angle X-ray Scattering: an Advanced Scattering Technique for the Investigation of Nanostructured Polymer Films. *Anal. Bioanal. Chem.* **2003**, *376*, 3−10.
(48) Seo, M. A.; Yim, J. H.; Ahn, Y. H.; Rotermund, F.; Kim, D. S.; Lee, S.; Lim, H. Terahertz Electromagnetic Interference Shielding Using Single-Walled Carbon Nanotube Flexible Films. *Appl. Phys. Lett.* **2008**, *93*, 231905.
(49) Nardes, A. M.; Kemerink, M.; Janssen, R. A. J.; Bastiaansen, J. A. M.; Kiggen, N. M. M.; Langeveld, B. M. W.; Van Breemen, A. J. J. M.; De Kok, M. M. Microscopic Understanding of the Anisotropic Conductivity of PEDOT:PSS Thin Films. *Adv. Mater.* **2007**, *19*, 1196−1200.
(50) Müller-Buschbaum, P.; Bauer, E.; Maurer, E.; Roth, S. V.; Gehrke, R.; Burghammer, M.; Riekel, C. Large-scale and Local-scale Structures in Polymer-blend Films: a Grazing-incidence Ultra-small-angle X-ray Scattering and Sub-microbeam Grazing-incidence Small-angle X-ray Scattering Investigation. *J. Appl. Crystallogr.* **2007**, *40*, S341−S345.
(51) Hamilton, W. A. Conformation, Directed Self-assembly and Engineered Modification: Some Recent Near Surface Structure Determinations by Grazing Incidence Small Angle X-ray and Neutron Scattering. *Curr. Opin. Colloid. Polym. Sci.* **2005**, *9*, 390−395.
(52) Müller-Buschbaum, P. The Active Layer Morphology of Organic Solar Cells Probed with Grazing Incidence Scattering Techniques. *Adv. Mater.* **2014**, *26*, 7692−7709.
(53) Renaud, G.; Lazzari, R.; Leroy, F. Probing Surface and Interface Morphology with Grazing Incidence Small Angle X-Ray Scattering. *Surf. Sci. Rep.* **2009**, *64*, 255−380.
(54) Hexemer, A.; Müller-Buschbaum, P. Advanced Grazing-Incidence Techniques for Modern Soft-Matter Materials Analysis. *IUCrJ* **2015**, *2*, 106−125.
(55) Sarkar, K.; Rawolle, M.; Herzig, E. M.; Wang, W.; Buffet, A.; Roth, S. V.; Müller-Buschbaum, P. Custom-Made Morphologies of ZnO Nanostructured Films Templated by a Poly(styrene-*block*-ethylene oxide) Diblock Copolymer Obtained by a Sol−Gel Technique. *ChemPhysChem* **2013**, *6*, 1414−1424.
(56) Guo, S.; Herzig, E. M.; Naumann, A.; Tainter, G.; Perlich, J.; Müller-Buschbaum, P. Influence of Solvent and Solvent Additive on the Morphology of PTB7 Films Probed via X-ray Scattering. *J. Phys. Chem. B* **2014**, *118*, 344−350.
(57) Salditt, T.; Metzger, T. H.; Peisl, J.; Reinker, B.; Moske, M.; Samwer, K. Determination of the Height-Height Correlation Function of Rough Surfaces from Diffuse X-Ray Scattering. *Europhys. Lett.* **1995**, *32*, 331−336.
(58) Yoneda, Y. Anomalous Surface Reflection of X Rays. *Phys. Rev.* **1963**, *131*, 2010−2013.
(59) Rueda, D. R.; Martin-Fabiani, I.; Soccio, M. A. N.; Perez-Murano, F.; Rebollar, E.; Garcia-Gutierrez, C.; Castillejo, M.; Ezquerra, T. A. Grazing-Incidence Small-Angle X-Ray Scattering of Soft and Hard Nanofabricated Gratings. *J. Appl. Crystallogr.* **2012**, *45*, 1038−1045.
(60) Chourou, S. T.; Sarje, A.; Li, X. S.; Chanb, E. R.; Hexemer, A. *HipGISAXS*: A High-Performance Computing Code for Simulating Grazing-Incidence X-ray Scattering Data. *J. Appl. Crystallogr.* **2013**, *46*, 1781−1795.

DOI: 10.1021/acsami.5b01327
ACS Appl. Mater. Interfaces 2015, 7, 8789−8797